

---

# Sketchy Empirical Natural Gradient Methods for Deep Learning

---

**Minghan Yang, Dong Xu, Yongfeng Li**  
 Beijing International Center for Mathematical Research,  
 Peking University, China  
 {yangminghan, taroxd, yongfengli}@pku.edu.cn

<b>Zaiwen Wen</b> Beijing International Center for Mathematical Research, Peking University, China wenzw@pku.edu.cn	<b>Mengyun Chen</b> Huawei Technologies Co. Ltd China chenmengyun1@huawei.com
--	--

## Abstract

In this paper, we develop an efficient sketchy empirical natural gradient method for large-scale finite-sum optimization problems from deep learning. The empirical Fisher information matrix is usually low-rank since the sampling is only practical on a small amount of data at each iteration. Although the corresponding natural gradient direction lies in a small subspace, both the computational cost and memory requirement are still not tractable due to the curse of dimensionality. We design randomized techniques for different neural network structures to resolve these challenges. For layers with a reasonable dimension, a sketching can be performed on a regularized least squares subproblem. Otherwise, since the gradient is a vectorization of the product between two matrices, we apply sketching on low-rank approximation of these matrices to compute the most expensive parts. Global convergence to stationary point is established under some mild assumptions. Numerical results on deep convolution networks illustrate that our method is quite competitive to the state-of-the-art methods such as SGD and KFAC.

## 1 Introduction

Deep learning [4, 6, 14, 21, 23] makes a breakthrough and holds great promise in many applications. Developing efficient and robust deep learning optimization methods is an urgent need from end users. The goal of deep learning is to find a fair good decision variable  $\theta \in \mathbb{R}^n$  so that the output of the network  $f(x, \theta)$  matches the true target  $y$ . Specifically, for a given dataset  $\{x_i, y_i\}_{i=1}^N$ , we consider the following empirical risk minimization problem with a loss function  $\psi(x, y, \theta) = -\log(p(y|x, \theta))$ :

$$\min_{\theta \in \mathbb{R}^n} \Psi(\theta) = \frac{1}{N} \sum_{i=1}^N \psi_i(\theta) = \frac{1}{N} \sum_{i=1}^N -\log(p_i(\theta)), \quad (1)$$

where  $\psi_i(\theta) = \psi(x_i, y_i, \theta)$ ,  $p_i(\theta) = p(y_i|x_i, \theta)$  and  $p$  is a distribution learned by the current network.

The basic and most popular optimization methods in deep learning are first-order type methods, such as SGD [19], AdaGrad [5], Adam [13] and etc. They are easy to implement but suffer a slow convergence rate and generalization gap in distributed large-batch training [12, 22]. Second-order type methods enjoy better convergence properties and exhibit a good potential in distributed large-batch training [17], but suffer a high computational cost at each iteration. They leverage the curvature information in different ways. The natural gradient method [1] corrects the gradient according to the

local KL-divergence surface. An online approximation to the natural gradient direction is used in the TONGA method [20]. The online Newton step algorithm [9] uses the empirical fisher information matrix (EFIM) and the authors analyze the convergence properties in the online learning setting. The Fisher Information Matrix (FIM) is integrated naturally with a practical Levenberg-Marquardt framework [18] and the direction can be economically computed by using the Sherman-Morrison-Woodbury (SMW) formula. The KFAC method [16] based on independence assumptions approximates the FIM by decomposing the large matrix into a Kronecker product between two smaller matrices each layer. A recursive block-diagonal approximation to the Gauss-Newton matrix is studied in [2] and each block is Kronecker factored and can be computed by a single backward pass. The Shampoo method [8] maintains a “structured” matrix which is implicitly used to precondition the gradient. By using fast Hessian matrix-vector products, the Hessian-free method [15] uses the conjugate-gradient method to compute the corresponding direction. The CURVEBALL method [11] takes the curvature information with two additional forward-mode automatic differentiation operations over the network.

In this paper, we develop a novel **Sketchy Empirical Natural Gradient (SENG)** method. The original empirical natural gradient method (ENG) uses the EFIM but the cost is not tractable due to the curse of dimensionality. Our SENG method utilizes randomized techniques to reduce the computational complexity and memory requirement. Since the EFIM is usually low-rank subject to the sampling costs, the search direction is actually a linear combination of the subsampled gradients where the coefficients are determined by a regularized least squares subproblem. For layers with a reasonable dimension, we construct a much smaller subproblem by sketching on the subsampled gradients. Otherwise, since the gradient is a vectorization of the product between two matrices, we first take a low-rank approximation to these matrices and then use randomized algorithms to approximate the expensive operations. Global convergence is established under some mild assumptions. Numerical comparisons with the state-of-the-art methods demonstrate the competitiveness of our method on deep learning problems.

## 2 The Empirical Fisher Information Matrix

The FIM of the loss in (1) is  $\mathbb{E}_{p(y|x,\theta)} \nabla \psi(\theta) \nabla \psi(\theta)^\top$ , where the expectation is taken over the distribution learned by the current neural network. Since sampling from the current distribution  $p(y|x, \theta)$  is costly, we consider using the subsampled EFIM as our curvature matrix. Given a mini-batch  $S \subset \{1, 2, \dots, N\}$  with a sample size  $\varrho = |S|$ , the subsampled EFIM can be represented as follows:

$$M_S(\theta) = \frac{1}{\varrho} \sum_{i \in S} \nabla \psi_i(\theta) \nabla \psi_i(\theta)^\top. \quad (2)$$

The subsampled EFIM (2) is a summation of a few rank-one matrices and is low-rank if  $n \gg \varrho$ . In this paper, we consider a convolutional neural network with  $L$  layers. The gradient with respect to  $\psi_i$  at layer  $l$  can be obtained by the back-propagation process and written as a vectorization of matrix-matrix multiplication [7]

$$u_i^l(\theta) = \text{vec}(\hat{G}_i^l(\theta)(\hat{A}_i^l(\theta))^\top), \quad (3)$$

where  $\hat{G}_i^l(\theta) \in \mathbb{R}^{n_G^l \times \kappa^l}$ ,  $\hat{A}_i^l(\theta) \in \mathbb{R}^{n_A^l \times \kappa^l}$ ,  $n^l = n_G^l \cdot n_A^l$  and  $n^l$  is the number of parameters in the  $l$ -th layer. The per-sample gradient is a concatenation of  $L$  sub-vectors:

$$u_i(\theta) = [(u_i^1(\theta))^\top, \dots, (u_i^l(\theta))^\top, \dots, (u_i^L(\theta))^\top]^\top := \nabla \psi_i(\theta) \in \mathbb{R}^n.$$

We denote the collection of gradients with respect to the sample set  $S$  as  $U_S(\theta) = \frac{1}{\sqrt{\varrho}}[u_1(\theta), u_2(\theta), \dots, u_\varrho(\theta)] \in \mathbb{R}^{n \times \varrho}$  and the collection of gradients with respect to  $l$ -th layer as  $U_S^l(\theta) = \frac{1}{\sqrt{\varrho}}[u_1^l(\theta), u_2^l(\theta), \dots, u_\varrho^l(\theta)] \in \mathbb{R}^{n^l \times \varrho}$ . Hence, the subsampled EFIM matrix  $M_S(\theta)$  and the mini-batch gradient  $g_S(\theta)$  can be written as:

$$M_S(\theta) = \frac{1}{\varrho} \sum_{i \in S} u_i(\theta) u_i(\theta)^\top = U_S(\theta) U_S(\theta)^\top, \quad g_S(\theta) = \frac{1}{\varrho} \sum_{i \in S} u_i(\theta). \quad (4)$$

Note that the subscript  $S$  is dropped if we do not emphasize the sample set and  $\theta$  is omitted if no confusion can arise. Throughout this paper, the layer number is expressed by the superscripts.

### 3 The Sketchy Empirical Natural Gradient Methods

We first describe a second-order framework for the finite-sum problem (1). At the  $k$ -th iteration, a regularized quadratic minimization problem at the point  $\theta_k$  is constructed as follows:

$$\min_d F_k(d) = \Psi_k + g_k^\top d + \frac{1}{2} d^\top (B_k + \lambda_k I) d, \quad (5)$$

where  $\Psi_k = \Psi(\theta_k)$ ,  $g_k = g_{S_k}(\theta_k)$  is the mini-batch gradient,  $B_k$  is an approximation to the Hessian matrix of  $\Psi$  at  $\theta_k$  and  $\lambda_k$  is a regularization parameter to make  $B_k + \lambda_k I$  positive definite.

To reduce the computational cost, we use the following block diagonal matrix:

$$B_k = \text{diag}\{U_k^1(U_k^1)^\top, \dots, U_k^L(U_k^L)^\top\},$$

where  $U_k^l = U_{S_k}^l(\theta_k)$ . Hence,  $B_k$  is positive semi-definite. By minimizing the quadratic function (5), we obtain a direction  $d_k := [(d_k^1)^\top, \dots, (d_k^L)^\top]^\top$ , where

$$d_k^l = -(U_k^l(U_k^l)^\top + \lambda_k I)^{-1} g_k^l. \quad (6)$$

Then we set  $\theta_{k+1} = \theta_k + \alpha_k d_k$ , where  $\alpha_k$  is the step size. Since the formulations of the directions  $d_k^l$  (6) for all layers are identical, we next only focus on a single layer and drop the explicit layer indices and the iteration number  $k$  if no confusion can arise. Hence,  $n^l$  and  $U_k^l$  are written as  $n$  and  $U$  for simplicity.

#### 3.1 Direction in a Low-rank Subspace

By using the SMW formula, the direction in (6) actually is:

$$d = -ag + aUb, \quad (7)$$

where  $a = \frac{1}{\lambda}$  is a scalar and

$$b = (\lambda I + U^\top U)^{-1}(U^\top g) \in \mathbb{R}^q. \quad (8)$$

Therefore,  $d$  is located in a small subspace  $\text{span}\{g, u_1, u_2, \dots, u_\varrho\}$  and is a combination of the subsampled gradients  $g$  and  $U$ . The complexity of calculating the direction is reduced from  $O(n^3)$  to  $O(\varrho^3 + \varrho^2 n)$  by (7). The main cost is  $O(n\varrho^2)$  from the computation of the coefficients  $b$ . Note that the number of parameters in a convolution layer is over **1.3 million** in the ResNet18 [10] on the dataset CIFAR10. Therefore, both the computational cost and memory requirement of  $U$  can not be ignored due to the curse of dimensionality.

#### 3.2 Sketching on a Regularized Least Squares Subproblem

We next use a sketching method to reduce the computational cost of  $b$ . Our key observation is that the vector  $b$  in (7) is the solution of the following regularized least squares problem:

$$\min_{b \in \mathbb{R}^q} \|Ub - g\|^2 + \lambda \|b\|_2^2. \quad (9)$$

We reduce the scale of the subproblem by the sketching method. Denote  $\Xi = \Omega U$ ,  $\xi = \Omega g$ , where  $\Omega \in \mathbb{R}^{q \times n}$  is a sketching matrix ( $q \ll n$ ). The subproblem is modified to:

$$\min_{\hat{b} \in \mathbb{R}^q} \|\Omega U \hat{b} - \Omega g\|^2 + \lambda \|\hat{b}\|_2^2 = \|\Xi \hat{b} - \xi\|^2 + \lambda \|\hat{b}\|_2^2. \quad (10)$$

The solution of the problem (10) is

$$\hat{b} = (\lambda I + \Xi^\top \Xi)^{-1} \Xi^\top \xi. \quad (11)$$

Hence, the direction is changed to:

$$\hat{d} = -\frac{1}{\lambda}g + \frac{1}{\lambda}U\hat{b}. \quad (12)$$

Replacing (9) by (10), the complexity of calculating the coefficients is reduced from  $O(\varrho^2 n)$  to  $O(\varrho^2 q)$ .

**Construction of  $\Omega$ .** We consider random row samplings where the rows of  $\Omega_{i,:}$ ,  $i = 1, 2, \dots, q$ , are independent and sampled from

$$\omega \leftarrow \frac{e_i^\top}{p_i}, i = 1, 2, \dots, n, \quad (13)$$

where  $\{p_j\}$  are given sampling probabilities. Two common strategies are listed below:

- Uniform sampling: All  $p_i$  are the same and  $p_i = \frac{1}{n}$ ,  $\forall i = 1, 2, \dots, n$ .
- Leverage score sampling: Each  $p_i$  is proportional to the row norm squares  $\|U_{i,:}\|_2^2$ , where  $U_{i,:}$  is the  $i$ -th row of  $U$ , that is,  $p_i = \frac{\|U_{i,:}\|_2^2}{\sum_{i=1}^n \|U_{i,:}\|_2^2}$ .

Our experiments show the kinds of the sketching methods do not affect the performance very much.

### 3.3 Implicit Computation and Storage of $U$ to Reduce Complexity

Although the computational complexity is reduced by sketching, the memory consumption in (7) is still large. In this part, we combine sketching methods with the structure of the gradient to reduce the memory usage. We first assume that each element of  $U_S$  can be approximated as follows:

$$u_i = \text{vec}(\hat{G}_i \hat{A}_i^\top) \approx \text{vec}(G_i A_i^\top) = \sum_{j=1}^r a_{ij} \otimes g_{ij}, \quad (14)$$

where  $G_i = [g_{i1}, \dots, g_{ir}] \in \mathbb{R}^{n_G \times r}$ ,  $A_i = [a_{i1}, \dots, a_{ir}] \in \mathbb{R}^{n_A \times r}$  and  $r < \kappa$ . The approximation (14) can be achieved by computing a partial SVD of  $\hat{G}_i$ , i.e.,

$$\hat{G}_i \approx N_{G_i} \Sigma_{G_i} V_{G_i},$$

where  $N_{G_i} \in \mathbb{R}^{n_G \times r}$ ,  $\Sigma_{G_i} \in \mathbb{R}^{r \times r}$  and  $V_{G_i} \in \mathbb{R}^{r \times \kappa}$ . Hence, (14) can be obtained by setting  $G_i = N_{G_i} \Sigma_{G_i}$  and  $A_i = \hat{A}_i V_{G_i}^\top$ . These two matrices can be constructed in a similar fashion if a low-rank approximation to  $\hat{A}_i$  is available. The partial SVD can be obtained by cheap randomized SVD methods. Note that the above scheme is not needed when  $\kappa$  is small enough.

We next describe sketching methods to compute  $U^\top z$ ,  $U^\top U$  and  $U c$  for any vector  $z, c$  by using (14). Denote

$$\tilde{A} = [A_1, A_2, \dots, A_\varrho] \in \mathbb{R}^{n_A \times r\varrho}, \quad \tilde{G} = [G_1, G_2, \dots, G_\varrho] \in \mathbb{R}^{n_G \times r\varrho}. \quad (15)$$

When  $n_A$  or  $n_G$  is large, we sample the rows of  $\tilde{G}$  and  $\tilde{A}$  with two sketching matrices  $\Omega_G \in \mathbb{R}^{\zeta_G \times n_G}$  and  $\Omega_A \in \mathbb{R}^{\zeta_A \times n_A}$ . Hence, we obtain

$$\Xi_{\tilde{A}} = \Omega_A \tilde{A} = [\Xi_{A_1}, \dots, \Xi_{A_\varrho}], \quad \Xi_{\tilde{G}} = \Omega_G \tilde{G} = [\Xi_{G_1}, \dots, \Xi_{G_\varrho}], \quad (16)$$

where  $\Xi_{G_i} = \Omega_G G_i$  and  $\Xi_{A_i} = \Omega_A A_i$ . When  $n_A$  and  $n_G$  are already small enough, we simply let  $\Xi_{\tilde{A}} = \tilde{A}$  and  $\Xi_{\tilde{G}} = \tilde{G}$ .

**Computation of  $U^\top z$ .** We sketch the  $\text{mat}(z)$  with the same sketching matrices and define  $\Xi_z = \Omega_G \text{mat}(z) \Omega_A^\top$ , where  $\text{mat}(\cdot) : \mathbb{R}^n \rightarrow \mathbb{R}^{n_G \times n_A}$ . By using (14) and the randomized techniques, the  $i$ -th element of  $U^\top z$  can be approximated as:

$$u_i^\top z \approx \sum_{j=1}^r g_{ij}^\top \text{mat}(z) a_{ij} \quad (17)$$

$$\approx \text{elesum}((\Xi_z^\top \Xi_{G_i}) \odot (\Xi_{A_i})), \quad (18)$$

where  $\odot$  is the Hadamard product and  $\text{elesum}(X) = \sum_{ij} X_{ij}$ .

**Computation of  $U^\top U$ .** Similarly, the  $(i, j)$  element of  $U^\top U$  is approximated as:

$$(u_i)^\top u_j \approx \left( \sum_{k=1}^r a_{ik} \otimes g_{ik} \right)^\top \left( \sum_{k=1}^r a_{jk} \otimes g_{jk} \right) = \text{elesum}((A_i^\top A_j) \odot (G_i^\top G_j)) \quad (19)$$

$$\approx \text{elesum}((\Xi_{A_i}^\top \Xi_{A_j}) \odot (\Xi_{G_i}^\top \Xi_{G_j})). \quad (20)$$

**Computation of  $U_c$ .** To compute  $U_c$ , we first have to compute the per-sample gradient  $u_i$  for all  $i \in S$ , multiply them with corresponding  $c_i$  and finally sum them together (21):

$$U_c = \sum_{i \in S} u_i c_i \approx \sum_{i \in S} \text{vec}(G_i A_i^\top) c_i. \quad (21)$$

The process (21) is expensive since it requires the computation of  $\varrho$  matrix-matrix products and vectorizations as well. When the dimension  $n$  is large, the computational cost is not tractable. Alternatively, we assume  $A_i$  and  $G_i$  are independent and approximate  $U_c$  by the product between the weighted averages of  $G_i$  and  $A_i$  as follows:

$$U_c \approx \mathcal{C}_U(c) = \text{vec} \left( \sum_{i \in S} \sqrt{|c_i|} G_i \right) \left( \sum_{i \in S} \frac{c_i}{\sum_{i=1}^{\varrho} \sqrt{|c_i|}} A_i \right)^\top. \quad (22)$$

Therefore, an explicit calculation and storage of  $u_i$  is avoided, and only one matrix-matrix multiplication is needed. Let  $\mathcal{A}_{\Omega_A, \Omega_G, U}(z)$  and  $\mathcal{B}_{\Omega_A, \Omega_G, U}$  be the approximation of  $U^\top z$  by (18) and  $U^\top U$  by (20). Combining them with (22), the direction can be obtained as follows:

$$\hat{d} = -\frac{1}{\lambda} g + \mathcal{C}_U(\hat{b}), \quad (23)$$

where  $\hat{b} = (\mathcal{B}_{\Omega_A, \Omega_G, U} + \lambda I)^{-1} \mathcal{A}_{\Omega_A, \Omega_G, U}(g)$ . Note that (18) and (20) are equal to  $((\Omega_A \otimes \Omega_G)u_i)^\top ((\Omega_A \otimes \Omega_G)z)$  and  $((\Omega_A \otimes \Omega_G)u_i)^\top ((\Omega_A \otimes \Omega_G)u_j)$ , respectively. Therefore, the computation of  $\hat{b}$  here can be seen as a special case of (11) by choosing  $\Omega = (\Omega_A \otimes \Omega_G)$ . We summarize the computation of the direction  $\hat{d}$  in Algorithm 1.

---

**Algorithm 1:** The Computation of the Direction

---

1 **INPUT:** Curvature matrix update frequency  $T$ , threshold  $\mathcal{N}$  and regularization  $\lambda_k$ .  
 for layer  $l = 0, 1, \dots, L$  do  
 if  $n^l < \mathcal{N}$  then  
 if  $k \bmod T = 0$  then save  $U_k^l$ , else set  $U_k^l = U_{k-1}^l$ ;  
 Construct the sketching matrix  $\Omega_k^l$  by (13);  
 Solve the sketched least squares problem (10) and set  $\hat{d}_k^l$  by (12);  
 else  
 if  $k \bmod T = 0$  then update  $\tilde{A}_k^l, \tilde{G}_k^l$  by (15), else set  $\tilde{A}_k^l = \tilde{A}_{k-1}^l$  and  $\tilde{G}_k^l = \tilde{G}_{k-1}^l$ ;  
 Construct the sketching matrix  $(\Omega_G)_k^l$  and  $(\Omega_A)_k^l$  by (13);  
 Compute  $\hat{d}_k^l$  by (23);  
 7 **OUTPUT:**  $\hat{d}_k := [(\hat{d}_k^1)^\top, \dots, (\hat{d}_k^L)^\top]^\top$ .

---

### 3.4 Construction of $U_k$ by Historical Information

In the previous subsections, both  $g_k$  and  $U_k$  in (6) are computed on the same  $\theta_k$ . We next generalize  $U_k$  to be a buffer zone of the historical subsampled gradients in different ways.

**Limited-memory Historical Information.** Given the memory size  $p$  and a constant value  $\zeta \in (0, 1]$ , the buffer  $U_k \in \mathbb{R}^{n \times p}$  at the  $k$ -th iteration is:

$$U_k = \frac{1}{\sqrt{p}} [\zeta^{p-1} g_{k-p+1}, \dots, \zeta^0 g_k]. \quad (24)$$

When  $\zeta \in (0, 1)$ , we call the construction method the history information collection with decaying.

**Hybrid mini-batch and per-sample gradient.**  $U_k$  contains both the mini-batch gradients and per-sample gradients, that is,

$$U_k = \frac{1}{\sqrt{p}} [g_{k-v}, \dots, g_{k-1}, \nabla \psi_{i_1}(\theta_k), \dots, \nabla \psi_{i_{p-v}}(\theta_k)], \quad (25)$$

where  $i_1, i_2, \dots, i_{p-v} \in S_k$  are the indices and  $1 < v < p$ .

Table 1: A summary of the computational and memory complexity.

	Computational Cost	Memory Consumption
Low-rank Computation (7)	$\varrho^3 + \varrho^2 n$	$\varrho n$
Original LS (9)	$\varrho^2 n$	$\varrho n$
Sketchy LS (10)	$\varrho^2 q$	$\varrho n$
$U^\top z$	$\varrho n$	$\varrho n$
$U^\top z$ (17)	$n_A n_G \varrho r$	$(n_A + n_G) r \varrho$
Randomized $U^\top z$ (18)	$\zeta_A \zeta_G \varrho r$	$(\zeta_A + \zeta_G) r \varrho$
$U^\top U$	$\varrho^2 n$	$\varrho n$
$U^\top U$ (19)	$r^2 \varrho^2 (n_A + n_G)$	$(n_A + n_G) r \varrho$
Randomized $U^\top U$ (20)	$r^2 \varrho^2 (\zeta_A + \zeta_G)$	$(\zeta_A + \zeta_G) r \varrho$
$U_c$	$\varrho n$	$\varrho n$
$U_c$ (21)	$n_A n_G r \varrho$	$(n_A + n_G) r \varrho$
$U_c$ (22)	$n_A n_G r$	$(n_A + n_G) r \varrho$

We summarize our SENG in Algorithm 2.

---

**Algorithm 2:** The Sketchy Empirical Natural Gradient Methods

---

- 1 **INPUT:** Initial parameter  $\theta_1$ , step size  $\{\alpha_k\}$  and regularization  $\{\lambda_k\}$ .
- 2 **for**  $k = 1, \dots, T$  **do**
- 3     Choose the sample set  $S_k$  and compute  $g_k$  using (4);
- 4     Construct  $U_k$  by  $U_{S_k}$  or from historical information in Sec.3.4;
- 5     Compute the direction  $\hat{d}_k$  by Algorithm 1;
- 6     Set  $\theta_{k+1} = \theta_k + \alpha_k \hat{d}_k$ ;
- 7 **OUTPUT:**  $\theta_{T+1}$ .

---

### 3.5 Computational and Memory Complexity

In this subsection, we summarize computational cost and memory consumption of the methods discussed in subsections 3.2-3.3 in Table 1. We can observe that the randomized methods reduce the computational cost and memory usage.

## 4 Convergence Analysis

In this section, we consider the case where  $g_k$  is set to be the full gradient  $\nabla \Psi(\theta_k)$ . When  $g_k$  is the mini-batch gradient, similar convergence properties can be established by adding some standard stochastic assumptions. We assume the directions for all layers are obtained by the sketched subproblem (10) in Sec.3.2. Since the update rules for all layers are identical, we only consider on one layer and drop the layer indices. The main idea of our proof is to first estimate the error between  $d_k$  (7) and  $\hat{d}_k$  (12) and the descent of the function values, then balance them by choosing a suitable step size. We give some necessary assumptions below.

**Assumption 1.** *A.1  $\Psi$  is continuously differentiable on  $\mathbb{R}^n$  and is bounded from below. The gradient  $\nabla \Psi$  is Lipschitz continuous on  $\mathbb{R}^n$  with modulus  $L_\Psi \geq 1$ .*

*A.2 There exists positive constants  $h_1, h_2$  such that*

$$h_1 I \preceq (B_k + \lambda_k I) \preceq h_2 I$$

*for all  $k$ .*

**Assumption 2.** *Let  $\eta_k, \epsilon_k \in (0, 1)$ . Let  $v$  be any fixed vector and  $N_k \in \mathbb{R}^{n \times \rho_k}$  be an orthogonal basis for the column span of  $U_k$ , where  $\rho_k = \text{rank}(U_k)$ . Let  $\Omega_k \in \mathbb{R}^{q_k \times n}$  be a sketching matrix, where the sample size  $q_k$  depends on  $\eta_k, \epsilon_k$  and  $\delta_k$ . The following two assumptions hold for all  $k$  with a probability  $1 - \delta_k$ :*

$$B.1) \|N_k^\top \Omega_k^\top \Omega_k N_k - I\|_2 \leq \eta_k,$$

$$B.2) \|N_k^\top \Omega_k^\top \Omega_k v - N_k^\top v\|_2^2 \leq \epsilon_k \|v\|_2^2.$$

Assumptions A.1-A.2 are common in stochastic quasi-Newton type methods [3, 26, 27]. Assumptions B.1-B.2 are called subspace embedding property and matrix multiplication property, respectively and standard in related sketching methods [24, 25]. When the sample size  $q_k$  is large enough, Assumptions B.1 and B.2 will be satisfied, see [24, 25]. We next estimate the error between  $b_k$  (8) and  $\hat{b}_k$  (11).

**Lemma 3.** *Suppose that Assumptions A.2, B.1 and B.2 are satisfied with  $\eta_k$  and  $\epsilon_k$ . It holds*

$$\|b_k - \hat{b}_k\|_2 \leq \frac{1}{\sqrt{h_1}} \frac{\sqrt{\epsilon_k} + \eta_k}{1 - \eta_k} \|g_k\|_2 \quad (26)$$

with probability at least  $1 - \delta_k$ .

The proof of Lemma 3 is shown in Appendix. Next, we estimate the descent of the function value.

**Theorem 4.** *Suppose that Assumptions A.1-A.2, B.1-B.2 are satisfied and the step sizes  $\{\alpha_k\}$  satisfy  $\alpha_k \leq \min\{\frac{1}{2L_\Psi}, \frac{h_1^2}{2L_\Psi h_2}\}$ . Let  $\{\theta_k\}$  be generated by Algorithm 2 with  $\frac{\sqrt{\epsilon_k} + \eta_k}{\lambda_k(1 - \eta_k)} < \frac{-2\sqrt{\frac{h_2}{h_1}} + \sqrt{4\frac{h_2}{h_1} + \frac{2h_1}{h_2}}}{2h_1}$ . Then it holds*

$$\Psi(\theta_{k+1}) \leq \Psi(\theta_k) - \frac{\alpha_k}{4h_2} \|g_k\|_2^2$$

with probability at least  $1 - \delta_k$ .

The proof of Theorem 4 is shown in Appendix. We establish the global convergence as follows.

**Corollary 5.** *Suppose that the same assumptions hold as Theorem 4. If the step size  $\{\alpha_k\}$  further satisfies  $\sum_{k=1}^{\infty} \alpha_k = \infty$ , it holds*

$$\lim_{k \rightarrow \infty} \|g_k\|_2 = 0$$

with probability  $\Pi_{k=1}^{\infty} (1 - \delta_k)$ .

The proof of Corollary 5 is shown in Appendix.

## 5 Numerical Experiments

In this section, we report numerical results with an average of 5 different runs on the CIFAR10 dataset with the ResNet18 [10]. For a fair comparison, the batch size and the momentum are set to be 256 and 0.9, and we decrease the learning rate by 0.1 every 30 epochs for all methods. For KFAC and our methods, the frequency of updating the curvature matrix, the initial learning rate and the regularization parameters  $\lambda_k$  are set to be 50, 0.1 and  $0.8 \times 0.6^{\lfloor \text{epoch}/30 \rfloor}$ , respectively. Our codes are implemented in PyTorch and our experiments are run on one Tesla V100 GPU with 32GB memory.

**Different sketching on (10).** We first study the behavior of different randomized strategies on the subproblem (10) and assume that the directions in all layers are obtained by (12) to eliminate other factors. ENG computes the direction of each layer by (7). The variants of SENG by uniform/leverage score sampling with size 2048/8192 are called SENG-SU-2048, SENG-SU-8192, SENG-SN-2048 and SENG-SN-8192, respectively. The changes of the testing accuracy and training loss over time and testing accuracy over epoch for five methods are reported in Figure 1. Compared with ENG, the sketchy techniques accelerate the training time while all methods exhibit similar patterns in the curves with respect to epoch. In addition, the sampling sizes and the sampling types do not affect the performance much over epoch.

**Different constructions of  $U_k$ .** We show the performance of different construction methods of  $U_k$ . The directions in all layers are given by (12) with a sketching matrix that uniformly samples 8192 rows. We denote SENG-SU-8192 by SENG-S for simplicity and SENG with (25) by SENG-H. The variants of SENG with (24) are dubbed as SENG-A if  $\zeta = 1$  and SENG-D if  $\zeta = 0.98$ . The comparison for different variants is reported in Figure 2. We can see that SENG-S is better on testing accuracy than other variants while the behavior of all methods is similar on the training loss and training accuracy with respect to epoch.

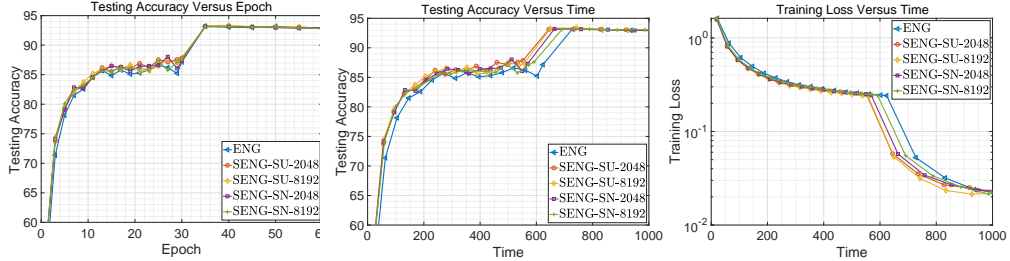


Figure 1: Comparison of different sketching variants of SENG.

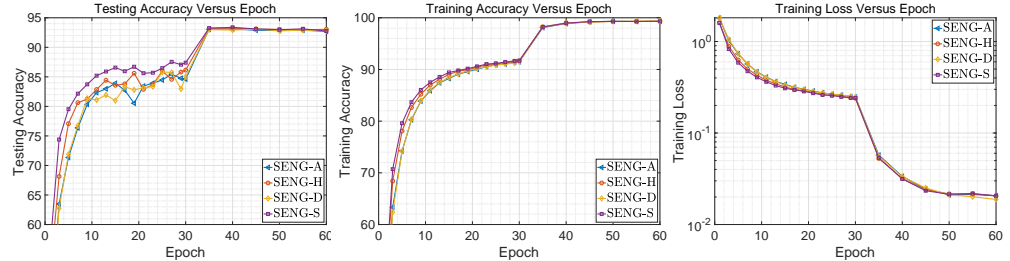


Figure 2: Comparison of different methods of constructing  $U_k$ .

**Comparison with SGD and KFAC.** Comparison results between our variants and the state-of-the-art methods are reported in this part. SENG is implemented as Algorithm 2 where  $\mathcal{N} = 10^6$  and  $U_k = U_{S_k}$ . Moreover, we use uniform sampling with the sample size 8192 in (10) and  $\zeta_A^l$  and  $\zeta_G^l$  are set to be 128 when both  $n_A^l$  and  $n_G^l$  are larger than 128 in (16). For SGD, the learning rate  $\alpha_0$  is carefully tuned to be 0.12.

The changes of the testing and training accuracy over epoch and testing accuracy over time are reported in Figure 3. A summary of the computational results is further given in Table 5. In terms of the time consumption per epoch, SENG is only slower than SGD, and faster than KFAC and ENG due to different randomized strategies on different layers. On the other hand, the best testing accuracy of SENG is only slightly worse than KFAC but better than SGD. In particular, SENG attains a good testing accuracy of 93% in 530 seconds while KFAC and SGD need 577 and 542 seconds, respectively. The results also illustrate that our sketchy methods indeed accelerate ENG with similar generalization abilities.

Table 2: A summary of the computational results on ResNet18.

	SGD	KFAC	ENG	SENG-S	SENG
Best Test Acc	93.9%	94.6%	94.3%	94.3%	94.3%
Time Per Epoch	12.02 s	18.55 s	20.78 s	18.51 s	16.53 s
Time (90%)	374 s	577 s	644 s	575 s	513 s
Time (92%)	386 s	577 s	644 s	575 s	513 s
Time (93%)	542 s	577 s	665 s	594 s	530 s
Time (94%)	NaN	670 s	1351 s	1186 s	1041 s

## 6 Conclusion

In this paper, we develop efficient sketching techniques for the empirical natural gradient method for deep learning problems. Since the EFIM is usually low-rank, the corresponding direction is actually a linear combination of the subsampled gradients based on the SMW formula. For layers whose number of parameters is not huge, we construct a much smaller least squares problem by sketching on the subsampled gradients. Otherwise, the quantities in the SMW formula is computed by using the matrix-matrix representation of the gradients. We first approximate them by low-rank matrices, then use sketching methods to compute the expensive parts. Global convergence is guaranteed under some standard assumptions. Our numerical results show that the empirical natural gradient method

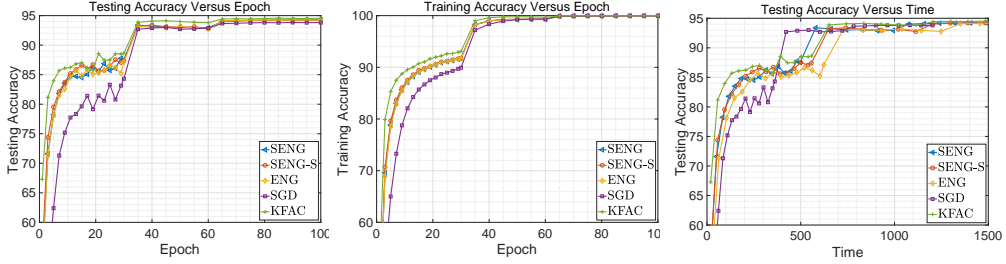


Figure 3: Comparison results with SGD and KFAC.

with randomized techniques can be quite competitive with the state-of-the-art methods such as SGD and KFAC. In the future, we will implement our method on MindSpore<sup>1</sup>, a unified training and inference framework for device, edge and cloud in Huawei’s full-stack, all-scenario AI portfolio.

## Source Codes

The PYTHON codes for SENG are available at <https://github.com/taroxd/seng>.

## References

- [1] Shun-ichi Amari. Neural learning in structured parameter spaces-natural riemannian gradient. In *Advances in neural information processing systems*, pages 127–133, 1997.
- [2] Aleksandar Botev, Hippolyt Ritter, and David Barber. Practical Gauss-Newton optimisation for deep learning. In *International Conference on Machine Learning*, pages 557–565, 2017.
- [3] R. H. Byrd, S. L. Hansen, Jorge Nocedal, and Y. Singer. A stochastic quasi-Newton method for large-scale optimization. *SIAM Journal on Optimization*, 26(2):1008–1031, 2016.
- [4] Li Deng and Dong Yu. Deep learning: Methods and applications. *Found. and Trends® Signal Process.*, 7(3–4):197–387, June 2014.
- [5] John Duchi, Elad Hazan, and Yoram Singer. Adaptive subgradient methods for online learning and stochastic optimization. *Journal of machine learning research*, 12(Jul):2121–2159, 2011.
- [6] Ian Goodfellow, Yoshua Bengio, and Aaron Courville. *Deep Learning*. MIT Press, 2016.
- [7] Roger Grosse and James Martens. A kronecker-factored approximate fisher matrix for convolution layers. In *International Conference on Machine Learning*, pages 573–582, 2016.
- [8] Vineet Gupta, Tomer Koren, and Yoram Singer. Shampoo: Preconditioned stochastic tensor optimization. In *International Conference on Machine Learning*, pages 1842–1850, 2018.
- [9] Elad Hazan, Amit Agarwal, and Satyen Kale. Logarithmic regret algorithms for online convex optimization. *Machine Learning*, 69(2-3):169–192, 2007.
- [10] Kaiming He, Xiangyu Zhang, Shaoqing Ren, and Jian Sun. Deep residual learning for image recognition. In *IEEE Conference on Computer Vision and Pattern Recognition*, pages 770–778, 2016.
- [11] João F Henriques, Sébastien Ehrhardt, Samuel Albanie, and Andrea Vedaldi. Small steps and giant leaps: Minimal newton solvers for deep learning. In *IEEE International Conference on Computer Vision*, pages 4763–4772, 2019.
- [12] Nitish Shirish Keskar, Dheevatsa Mudigere, Jorge Nocedal, Mikhail Smelyanskiy, and Ping Tak Peter Tang. On large-batch training for deep learning: Generalization gap and sharp minima. In *5th International Conference on Learning Representations, ICLR 2017, Toulon, France, April 24-26, 2017, Conference Track Proceedings*. OpenReview.net, 2017.

<sup>1</sup><https://gitee.com/mindspore/>

- [13] Diederik P Kingma and Jimmy Ba. Adam: A method for stochastic optimization. *arXiv preprint arXiv:1412.6980*, 2014.
- [14] Yann LeCun, Yoshua Bengio, and Geoffrey Hinton. Deep learning. *Nature*, 521:436–444, 2015.
- [15] James Martens. Deep learning via Hessian-free optimization. In *International Conference on Machine Learning*, pages 735–742, 2010.
- [16] James Martens and Roger Grosse. Optimizing neural networks with kronecker-factored approximate curvature. In *International conference on machine learning*, pages 2408–2417, 2015.
- [17] Kazuki Osawa, Yohei Tsuji, Yuichiro Ueno, Akira Naruse, Rio Yokota, and Satoshi Matsuoka. Large-scale distributed second-order optimization using kronecker-factored approximate curvature for deep convolutional neural networks. In *IEEE Conference on Computer Vision and Pattern Recognition*, pages 12359–12367, 2019.
- [18] Yi Ren and Donald Goldfarb. Efficient subsampled gauss-newton and natural gradient methods for training neural networks. *arXiv preprint arXiv:1906.02353*, 2019.
- [19] Herbert Robbins and Sutton Monro. A stochastic approximation method. *Ann. Math. Stat.*, 22:400–407, 1951.
- [20] Nicolas L Roux, Pierre-Antoine Manzagol, and Yoshua Bengio. Topmoumoute online natural gradient algorithm. In *Advances in neural information processing systems*, pages 849–856, 2008.
- [21] Jürgen Schmidhuber. Deep learning in neural networks: An overview. *Neural Networks*, 61:85–117, 2015.
- [22] Christopher J Shallue, Jaehoon Lee, Joseph Antognini, Jascha Sohl-Dickstein, Roy Frostig, and George E Dahl. Measuring the effects of data parallelism on neural network training. *Journal of Machine Learning Research*, 20:1–49, 2019.
- [23] Karen Simonyan and Andrew Zisserman. Very deep convolutional networks for large-scale image recognition. In *International Conference on Learning Representations*, 2015.
- [24] Shusen Wang, Alex Gittens, and Michael W. Mahoney. Sketched ridge regression: Optimization perspective, statistical perspective, and model averaging. *J. Mach. Learn. Res.*, 18(1):8039–8088, January 2017.
- [25] Shusen Wang, Luo Luo, and Zhihua Zhang. Spd matrix approximation via column selection: Theories, algorithms, and extensions. *J. Mach. Learn. Res.*, 17(1):1697–1745, January 2016.
- [26] Xiao Wang, Shiqian Ma, Donald Goldfarb, and Wei Liu. Stochastic Quasi-Newton Methods for Nonconvex Stochastic Optimization. *SIAM Journal on Optimization*, 27(2):927–956, 2017.
- [27] Minghan Yang, Andre Milzarek, Zaiwen Wen, and Tong Zhang. A stochastic extra-step quasi-newton method for nonsmooth nonconvex optimization. *ArXiv:1910.09373*, 2019.

# Appendix

## Proof of Lemma 3

*Proof.* The SVD decomposition of  $U_k$  is:  $U_k = N_k \Sigma_k V_k$ , where  $N_k \in \mathbb{R}^{n \times \rho_k}$ ,  $\Sigma_k \in \mathbb{R}^{\rho_k \times \rho_k}$ ,  $V_k \in \mathbb{R}^{\rho_k \times \rho}$  and  $\rho_k$  is the rank of  $U_k$ . Let  $g_k^\perp = g_k - U_k U_k^\dagger g_k = g_k - N_k N_k^\top g_k$ , where  $U_k^\dagger$  is the pseudoinverse of  $U_k$ . By the definition in (8) and (11),

$$b_k = (\lambda_k I + U_k^\top U_k)^{-1} (U_k^\top g_k) \text{ and } \hat{b}_k = (\lambda_k I + U_k^\top \Omega_k^\top \Omega_k U_k)^{-1} (U_k^\top \Omega_k^\top \Omega_k g_k),$$

we have:

$$\begin{aligned} & (\lambda_k I + U_k^\top \Omega_k^\top \Omega_k U_k)(\hat{b}_k - b_k) \\ &= U_k^\top \Omega_k^\top \Omega_k g_k^\perp + U_k^\top \Omega_k^\top \Omega_k U_k U_k^\dagger g_k - (\lambda_k I + U_k^\top \Omega_k^\top \Omega_k U_k)(\lambda_k I + U_k^\top U_k)^{-1} U_k^\top g_k \\ &= U_k^\top \Omega_k^\top \Omega_k g_k^\perp - \lambda_k U_k^\dagger g_k + (\lambda_k I + U_k^\top \Omega_k^\top \Omega_k U_k)(\lambda_k I + U_k^\top U_k)^{-1} [(\lambda_k I + U_k^\top U_k) U_k^\dagger g_k - U_k^\top g_k] \\ &= U_k^\top \Omega_k^\top \Omega_k g_k^\perp + \lambda_k (U_k^\top \Omega_k^\top \Omega_k U_k - U_k^\top U_k) (\lambda_k I + U_k^\top U_k)^{-1} U_k^\dagger g_k. \end{aligned} \tag{27}$$

The last equality follows from the fact that  $U_k^\top U_k U_k^\dagger g_k = U_k^\top g_k$ . By Assumption A.2, we know  $U_k^\top U_k + \lambda_k I$  is positive definite. We define:

$$(U_k^\top U_k + \lambda_k I)^{-1/2} (\lambda_k I + U_k^\top \Omega_k^\top \Omega_k U_k) (\hat{b}_k - b_k) := \Pi_k + \Delta_k, \tag{28}$$

where

$$\begin{aligned} \Pi_k &= (U_k^\top U_k + \lambda_k I)^{-1/2} U_k^\top \Omega_k^\top \Omega_k g_k^\perp = V_k^\top (\Sigma_k^2 + \lambda_k I)^{-1/2} \Sigma_k N_k^\top \Omega_k^\top \Omega_k g_k^\perp \\ \Delta_k &= \lambda_k (U_k^\top U_k + \lambda_k I)^{-1/2} (U_k^\top \Omega_k^\top \Omega_k U_k - U_k^\top U_k) (\lambda_k I + U_k^\top U_k)^{-1} U_k^\dagger g_k \\ &= \lambda_k V_k^\top \Sigma_k (\Sigma_k^2 + \lambda_k I)^{-1/2} (N_k^\top \Omega_k^\top \Omega_k N_k - I) (\Sigma_k^2 + \lambda_k I)^{-1} N_k^\top g_k. \end{aligned}$$

By Assumption B.1, it holds with probability  $1 - \delta_k$ :

$$(1 - \eta_k) I \preceq N_k^\top \Omega_k^\top \Omega_k N_k \preceq (1 + \eta_k) I.$$

By left multiplication  $V_k^\top \Sigma_k^\top$ , right multiplication  $\Sigma_k V_k$  to each matrix and using the fact  $N_k^\top N_k = I$ , we have

$$(1 - \eta_k) U_k^\top U_k \preceq U_k^\top \Omega_k^\top \Omega_k U_k \preceq (1 + \eta_k) U_k^\top U_k.$$

This implies

$$(1 - \eta_k) (\lambda_k I + U_k^\top U_k) \preceq (\lambda_k I + U_k^\top \Omega_k^\top \Omega_k U_k) \preceq (1 + \eta_k) (\lambda_k I + U_k^\top U_k).$$

Hence, we have

$$(1 - \eta_k) I \preceq (U_k^\top U_k + \lambda_k I)^{-1/2} (\lambda_k I + U_k^\top \Omega_k^\top \Omega_k U_k) (U_k^\top U_k + \lambda_k I)^{-1/2} \preceq (1 + \eta_k) I,$$

which yields

$$\begin{aligned} & \| (U_k^\top U_k + \lambda_k I)^{1/2} (\hat{b}_k - b_k) \|_2 \\ & \leq \| [(U_k^\top U_k + \lambda_k I)^{-1/2} (\lambda_k I + U_k^\top \Omega_k^\top \Omega_k U_k) (U_k^\top U_k + \lambda_k I)^{-1/2}]^{-1} \|_2 \| \Pi_k + \Delta_k \|_2 \\ & \leq \frac{1}{1 - \eta_k} \| \Pi_k + \Delta_k \|_2 \leq \frac{1}{1 - \eta_k} (\| \Pi_k \|_2 + \| \Delta_k \|_2). \end{aligned}$$

By using  $N_k^\top g_k^\perp = 0$  and Assumption B.2, we have with probability  $1 - \delta_k$ :

$$\begin{aligned} \| \Pi_k \|_2 & \leq \| (\Sigma_k^2 + \lambda_k I)^{-1/2} \Sigma_k \|_2 \| N_k^\top \Omega_k^\top \Omega_k g_k^\perp - N_k^\top g_k^\perp \|_2 \\ & \leq \sqrt{\epsilon_k} \| (\Sigma_k^2 + \lambda_k I)^{-1/2} \Sigma_k \|_2 \| g_k^\perp \|_2 \\ & \leq \sqrt{\epsilon_k} \| g_k^\perp \|_2 \leq \sqrt{\epsilon_k} \| g_k \|_2. \end{aligned} \tag{29}$$

By using Assumptions A.2 and B.1, we have with probability  $1 - \delta_k$ :

$$\begin{aligned}
\|\Delta_k\|_2 &\leq \lambda_k \|\Sigma_k(\Sigma_k^2 + \lambda_k I)^{-1/2}(N_k^\top \Omega_k^\top \Omega_k N_k - I)(\Sigma_k^2 + \lambda_k I)^{-1} N_k^\top g_k\|_2 \\
&\leq \lambda_k \eta_k \|\Sigma_k(\Sigma_k^2 + \lambda_k I)^{-1/2}\|_2 \|\Sigma_k^2 + \lambda_k I\|^{-1} \|N_k^\top g_k\|_2 \\
&\leq \eta_k \|\Sigma_k(\Sigma_k^2 + \lambda_k I)^{-1/2}\|_2 \|N_k^\top g_k\|_2 \\
&\leq \eta_k \|g_k\|_2.
\end{aligned} \tag{30}$$

By Assumption A.2 and combining (28), (30) and (29), we have

$$\|\hat{b}_k - b_k\|_2 \leq \frac{1}{\sqrt{h_1}} \frac{\sqrt{\epsilon_k} + \eta_k}{1 - \eta_k} \|g_k\|_2 \tag{31}$$

with probability  $1 - \delta_k$  and this completes the proof of Lemma 3.  $\square$

## Proof of Theorem 4

*Proof.* By the defintion (7) and (12), we have  $\hat{d}_k - d_k = \frac{1}{\lambda_k} U_k (\hat{b}_k - b_k)$ . Since  $\|U_k\|_2^2 \leq \|\lambda_k I + U_k U_k^\top\|_2 \leq h_2$ , we obtain  $\|U_k\|_2 \leq \sqrt{h_2}$ . It follows that

$$\|d_k - \hat{d}_k\|_2 \leq \sqrt{\frac{h_2}{h_1}} \frac{\sqrt{\epsilon_k} + \eta_k}{\lambda_k(1 - \eta_k)} \|g_k\|_2 = \sqrt{\frac{h_2}{h_1}} t_k \|g_k\|_2, \tag{32}$$

where  $t_k = \frac{\sqrt{\epsilon_k} + \eta_k}{\lambda_k(1 - \eta_k)}$ . It follows from Assumptions A.1-A.2 that

$$-h_1^{-1} \|g_k\|_2^2 \leq \langle g_k, d_k \rangle = \langle g_k, -(B_k + \lambda_k I)^{-1} g_k \rangle \leq -h_2^{-1} \|g_k\|_2^2 \tag{33}$$

and

$$\|d_k\|_2^2 = \|(B_k + \lambda_k I)^{-1} g_k\|_2^2 \leq h_1^{-2} \|g_k\|_2^2. \tag{34}$$

Combining (33), (34), (32) and Assumptions A.1, B.2, it holds with probability  $1 - \delta_k$ :

$$\begin{aligned}
\Psi(\theta_{k+1}) &\leq \Psi(\theta_k) + \langle g_k, \theta_{k+1} - \theta_k \rangle + \frac{L_\Psi}{2} \|\theta_{k+1} - \theta_k\|_2^2 \\
&\leq \Psi(\theta_k) + \left\langle g_k, \alpha_k (d_k + \hat{d}_k - d_k) \right\rangle + L_\Psi \alpha_k^2 \left[ \|d_k\|_2^2 + \|\hat{d}_k - d_k\|_2^2 \right] \\
&\leq \Psi(\theta_k) - (\alpha_k h_2^{-1} - L_\Psi \alpha_k^2 h_1^{-2}) \|g_k\|_2^2 + \alpha_k \sqrt{\frac{h_2}{h_1}} t_k \|g_k\|_2^2 + L_\Psi \alpha_k^2 \frac{h_2}{h_1} t_k^2 \|g_k\|_2^2 \\
&= \Psi(\theta_k) - \alpha_k \left( h_2^{-1} - L_\Psi \alpha_k h_1^{-2} - \sqrt{\frac{h_2}{h_1}} t_k - L_\Psi \alpha_k \frac{h_2}{h_1} t_k^2 \right) \|g_k\|_2^2.
\end{aligned} \tag{35}$$

If  $\alpha_k \leq \min\{\frac{1}{2L_\Psi}, \frac{h_1^2}{2L_\Psi h_2}\}$ , we have

$$\frac{1}{h_2} - L_\Psi \alpha_k \frac{1}{h_1^2} > \frac{1}{2h_2}.$$

If  $t_k < \frac{-2\sqrt{\frac{h_2}{h_1}} + \sqrt{4\frac{h_2}{h_1} + \frac{2h_1}{h_2}}}{2h_1}$ , we obtain

$$\left( h_2^{-1} - L_\Psi \alpha_k h_1^{-2} - \sqrt{\frac{h_2}{h_1}} t_k - L_\Psi \alpha_k \frac{h_2}{h_1} t_k^2 \right) > \frac{1}{2h_2} - \sqrt{\frac{h_2}{h_1}} t_k - \frac{1}{2} h_1 t_k^2 > \frac{1}{4h_2}. \tag{36}$$

Let  $\epsilon_k$  and  $\eta_k$  be small enough so that  $t_k$  is small. This can be achieved by choosing suitable sample sizes. Combining (36) and (35) yields

$$\Psi(\theta_{k+1}) \leq \Psi(\theta_k) - \frac{\alpha_k}{4h_2} \|g_k\|_2^2. \tag{37}$$

This completes the proof of Theorem 4.  $\square$

## Proof of Corollary 5

*Proof.* Define the corresponding events of Lemma 3 by  $\Gamma_k$ . Then, we have

$$\mathbb{P}(\Gamma_k) = 1 - \delta_k$$

and this implies  $\mathbb{P}(\cap_{k=1}^{\infty} \Gamma_k) = \prod_{k=1}^{\infty} (1 - \delta_k)$ . The deductions in the next are on the events  $\cap_{k=1}^{\infty} \Gamma_k$ . Summing over the inequality (37) gives

$$\sum_{k=1}^{\infty} \frac{\alpha_k}{4h_2} \|\Psi(\theta_k)\|_2^2 \leq \Psi(\theta_1) - \Psi^*. \quad (38)$$

Therefore, we have  $\sum_{k=1}^{\infty} \alpha_k \|\nabla \Psi(\theta_k)\|_2^2 < \infty$  and infer that  $\alpha_k \|\nabla \Psi(\theta_k)\|_2^2 \rightarrow 0$ ,  $k \rightarrow \infty$ . Since  $\sum_{k=1}^{\infty} \alpha_k = \infty$ , we can conclude that there is a subsequence  $\{o_i\}_i$  such that  $\{\|\nabla \Psi(\theta_{o_i})\|_2^2 \rightarrow 0\}$ , which is equivalent to

$$\lim_{k \rightarrow \infty} \inf \|\nabla \Psi(\theta_k)\|_2 = 0. \quad (39)$$

By Assumption A.2, (32) and (38), we obtain

$$\sum_{k=1}^{\infty} \alpha_k^{-1} \|\theta_{k+1} - \theta_k\|_2^2 = \sum_{k=1}^{\infty} \alpha_k \|d_k - d_k + \hat{d}_k\|_2^2 \leq \sum_{k=1}^{\infty} \alpha_k (h_1^{-2} + \frac{h_2}{h_1} t_k^2) \|\nabla \Psi(\theta_k)\|_2^2 < \infty. \quad (40)$$

The last inequality follows from the fact that  $t_k$  has an upper bound. Next, we prove the result by contradiction. Assume that there exists  $\epsilon > 0$  and two increasing sequences  $\{p_i\}_i$ ,  $\{q_i\}_i$  such that  $p_i < q_i$  and

$$\|\nabla \Psi(\theta_{p_i})\|_2 \geq 2\epsilon, \quad \|\nabla \Psi(\theta_{q_i})\|_2 < \epsilon, \quad \|\nabla \Psi(\theta_k)\|_2 \geq \epsilon,$$

for  $k = p_i + 1, \dots, q_i - 1$ . Thus, it follows that

$$\epsilon^2 \sum_{i=0}^{\infty} \sum_{k=p_i}^{q_i-1} \alpha_k \leq \sum_{i=0}^{\infty} \sum_{k=p_i}^{q_i-1} \alpha_k \|\nabla \Psi(\theta_k)\|_2^2 \leq \sum_{k=0}^{\infty} \alpha_k \|\nabla \Psi(\theta_k)\|_2^2 < \infty. \quad (41)$$

Setting  $\zeta_i = \sum_{k=p_i}^{q_i-1} \alpha_k$  implies  $\zeta_i \rightarrow 0$ . Then by the Hölder's inequality and (40), we obtain

$$\|\theta_{p_i} - \theta_{q_i}\|_2 \leq \sqrt{\zeta_i} \left[ \sum_{k=p_i}^{q_i-1} \alpha_k^{-1} \|\theta_{k+1} - \theta_k\|_2^2 \right]^{1/2} \rightarrow 0.$$

Due to the Lipschitz property of  $\nabla \Psi$ , we have  $\lim_{i \rightarrow \infty} \|\nabla \Psi(\theta_{p_i}) - \nabla \Psi(\theta_{q_i})\|_2 \rightarrow 0$ , which is a contradiction. This implies  $\lim_{k \rightarrow \infty} \|\nabla \Psi(\theta_k)\|_2 = 0$  with probability  $\prod_{k=1}^{\infty} (1 - \delta_k)$  and completes the proof.  $\square$